PHYSICAL REVIEW B **92**, 144416 (2015)

Spin-flop transition and magnetic phase diagram in $CaCo_2As_2$ revealed by torque measurements

W. Zhang,[1,2] K. Nadeem,[2,3,*] H. Xiao,[2,†] R. Yang,[2] B. Xu,[2] H. Yang,[1,4,‡] and X. G. Qiu[2]

[1]*College of Physics, Optoelectronics and Energy & Collaborative Innovation Center of Suzhou Nano Science and Technology, Soochow University, Suzhou 215006, China*

[2]*Beijing National Laboratory for Condensed Matter Physics, National Laboratory for Superconductivity, Institute of Physics, Chinese Academy of Sciences, P.O. Box 603, Beijing 100190, China*

[3]*Department of Physics, International Islamic University, Islamabad, Pakistan*

[4]*College of Science, Nanjing University of Aeronautics and Astronautics, Nanjing 211106, China*

(Received 30 March 2015; published 16 October 2015)

The magnetic properties of a $CaCo_2As_2$ single crystal are systematically studied by using dc magnetization and magnetic torque measurements. A paramagnetic to antiferromagnetic transition occurs at $T_N = 74$ K, with Co spins being aligned parallel to the c axis. For $H \parallel c$, a field-induced spin-flop transition was observed below T_N and a magnetic transition from antiferromagnetic to paramagnetic was inferred from the detailed analysis of magnetization and magnetic torque. Finally, we summarize the magnetic phase diagram of $CaCo_2As_2$ based on our results in the H-T plane.

DOI: 10.1103/PhysRevB.92.144416 PACS number(s): 75.30.Gw, 75.30.Kz, 75.50.Ee

I. INTRODUCTION

In an uniaxial low anisotropic antiferromagnet, a sufficiently strong magnetic field applied along the easy axis could induce a spin-flop (SF) transition [1]. This response to the magnetic field has been observed in many antiferromagnetic (AFM) materials, such as AFM semiconductors [2], organic magnets [3–5], organic superconductors [6], and nanomagnetic systems [7]. In recent decades, several magnetic studies in the materials with a layered $ThCr_2Si_2$ type (122) crystal structure have been reported [8–11], which again come to fore in recent research after the discovery of superconductivity in the 122 iron-based family [12,13]. The parent compounds of these iron-based superconductors (FeSCs) are found to be AFM. The AFM order can be suppressed via carrier doping (hole or electron) or by applying pressure, and superconductivity emerges in the vicinity of vanishing AFM order. The most striking feature of FeSCs is the coexistence of magnetism and superconductivity [14–16], which also differentiates them from cuprates. Analysis of the magnetic transitions and order in the parent compounds can contribute to an understanding of the pairing mechanism in high-T_c superconductors [17,18].

The $CaFe_2As_2$ parent compound is an interesting material, which shows a nonmagnetic collapsed tetragonal (cT) phase and pressure-induced superconductivity [19–22]. And it exhibits a combined structural and magnetic transition at 170 K [23]. Recently, it was reported that $CaCo_2As_2$, the complete replacement of Fe in $CaFe_2As_2$ by Co, exhibits remarkably different properties compared to $CaFe_2As_2$ [24,25]. $CaCo_2As_2$ showed an A-type AFM order with the Co spins oriented ferromagnetically within the ab plane and antiferromagnetically along the c axis. The AFM aligned Co spins can be flopped by applying a magnetic field along the c axis and eventually aligned along the direction of the applied field at a sufficiently strong magnetic field. Cheng *et al.* reported two successive SF transitions in $CaCo_2As_2$ with a Neel temperature $T_N = 76$ K [24]. While Ying *et al.* reported single SF transition by using magnetization and electronic transport measurements [25], they also found that T_N is enhanced from 70 to 90 K and the SF field (H_{SF}) is suppressed with 10% Sr substitution on Ca sites ($Ca_{0.9}Sr_{0.1}Co_2As_2$). Quirinale *et al.* and Anand *et al.* studied the crystalline and magnetic structure of $CaCo_2As_2$ using x-ray diffraction and neutron diffraction analysis, respectively [26,27]. The results showed an A-type AFM structure, which is in accord with that reported by Cheng *et al.* [24] and Ying *et al.* [25]. Besides, they found that the actual composition of $CaCo_2As_2$ is $CaCo_{1.86}As_2$ due to 7% vacancies on the Co lattice sites. The discrepancy in the reports motivates us to perform further research about the magnetic transition in this interesting compound, $CaCo_2As_2$, by using a different technique, i.e., torque magnetometry, which is very sensitive to magnetic transitions.

In this study, we use dc magnetization and magnetic torque measurements to clarify the SF transition in $CaCo_2As_2$ in more detail. We have provided a direct comparison of magnetization measurements with torque magnetometry. Torque magnetometry measures the magnetic torque $\tau = \vec{M} \times \vec{B}$ experienced by a sample of magnetic moment $\vec{M}$ in an applied magnetic field $\vec{B}$. Compared to longitudinal magnetometry, torque magnetometry is more sensitive to detect the metamagnetism because the magnitude and direction of the magnetization can be extracted simultaneously [28,29]. Our results in the $CaCo_2As_2$ single crystal reveal an A-type AFM structure, a field-induced SF, and a magnetic transition from the AFM to paramagnetic (PM) state below T_N. Finally, we give a detailed magnetic phase diagram in the H-T plane of the $CaCo_2As_2$ single crystal.

II. EXPERIMENTAL DETAILS

The $CaCo_2As_2$ single crystals were grown using the CoAs self-flux method, as described elsewhere [21,30]. The crystal structure was investigated by x-ray diffraction (Rigaku

*kashif.nadeem@iiu.edu.pk
†hxiao@iphy.ac.cn
‡yanghao@nuaa.edu.cn

D/MAX-Ultima III) using Cu K_α ($\lambda = 0.154$ nm) radiation at ambient conditions. The actual elemental compositions were analyzed by inductively coupled plasma-atomic emission spectrometry (ICP-AES, IRIS Intrepid II XDL) and an energy-dispersive x-ray (EDX) detector using a Hitachi S-4800 scanning tunnel microscope. Magnetization measurements were done using a superconducting quantum interference device (SQUID, Quantum Design) and physical property measurement system (PPMS-9, Quantum Design). The magnetic torque was measured as a function of angle and magnetic field over a wide temperature range by using a piezoresistive magnetometry. In piezoresistive magnetometry, the torque lever chip together with a puck is mounted on a PPMS horizontal rotator. The sample is mounted on the center of the chip using Apiezon N grease. A wheatstone bridge circuit (integrated on the chip) detects the change in the resistance of the piezoresistors, produced by the different magnetic torque. The samples for all measurements presented here are from the same batch.

III. RESULTS AND DISCUSSION

A. Crystal structure and EDX, ICP-AES

Figure 1(a) shows a typical XRD θ-2θ scan of a $CaCo_2As_2$ single crystal. All of the indexed peaks are identified as the $ThCr_2Si_2$ body-centered tetragonal structure phase. The presence of only $(00l)$ reflection peaks indicates that the c axis is perpendicular to the crystal plane. The calculated lattice constant of the c axis comes out to be ~10.3 Å, close to the previous report, where $a = b = 3.9906(1)$ Å, $c = 10.2798(2)$ Å [26].

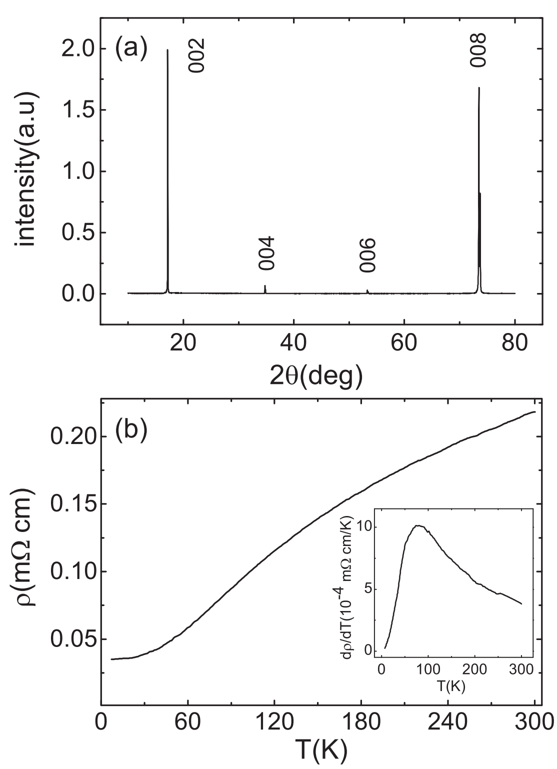

FIG. 1. (a) The typical XRD θ-2θ scan of a $CaCo_2As_2$ single crystal. (b) ρ vs T curve with $I \parallel ab$ at $H = 0$ T. Inset: $d\rho/dT$ vs T curve.

TABLE I. Actual composition of $CaCo_2As_2$ single crystal obtained from EDX and ICP-AES

	EDX			ICP-AES		
Sample No.	Ca	Co	As	Ca	Co	As
1	1	1.93	2.01	1.02	1.90	2
2	1	1.89	2.08	1	1.92	2
3	1	1.97	2.11	1	1.90	2

We have also done temperature-dependent resistivity $\rho(T)$ ($I \parallel ab$) measurements in the temperature range from 5 to 300 K [Fig. 1(b)]. There is no upturn resistivity associated with the AFM transition observed at T_N in the $\rho(T)$ curve, which is different from other 122 parent compounds such as $CaFe_2As_2$ and $BaFe_2As_2$ [12,13,31], where clear upturn resistivity was observed below their AFM transition temperature T_N. As shown in the inset of Fig. 1(b), a broad peak at 74 K is observed in $d\rho/dT$; such a broad peak in $d\rho/dT$ has been associated with the antiferromagnetic transition in Ref. [32].

Table I shows the results of EDX and ICP-AES measurements on three samples of $CaCo_2As_2$. From the EDX data, we conclude that the crystal has some vacancies on the Co sites; from the ICP-AES data, we estimate about a 5% vacancy on the Co sites, corresponding to the actual composition $CaCo_{1.9}As_2$, which is very close to the reported composition $CaCo_{1.86}As_2$ in Ref. [26].

B. Magnetization

Figure 2(a) shows the field-cooling (FC) magnetization in the temperature range from 5 to 300 K under magnetic field $H = 0.1$ T in $H \parallel c$ (diamonds) and $H \parallel ab$ (circles). For $H \parallel c$, the magnetization exhibits a sharp peak at 74 K and drops rapidly upon further cooling. For $H \parallel ab$, the magnetization exhibits a plateau below 74 K. We also give a Curie-Weiss fit ($\chi = \frac{C}{T-\theta}$, figure not shown) to the high-temperature parts of susceptibility ($150 \leqslant T \leqslant 300$ K), which gives a Weiss temperature $\theta_c = +82.5(3)$ K for $H \parallel c$ and $\theta_{ab} = +71.3(2)$ K for $H \parallel ab$. In general, a positive Weiss temperature means a ferromagnetic coupling between moments. Therefore, the above results may suggest that the Co spins are aligned antiferromagnetically along the c axis and ferromagnetically in the ab plane. The A-type AFM structure were also inferred and confirmed in previous reports [24–27]. The inset in Fig. 2(a) illustrates the unit cell of $CaCo_2As_2$ and the observed magnetic order of Co spins [26,27]. Both $M(T)$ and $\rho(T)$ measurements confirm the AFM transition at 74 K, which is close to the 76 K reported by Cheng *et al.* [24], but higher than the reported value of 52 K by Quirinale *et al.* [26]. We notice that there is controversy between the T_N values of Cheng *et al.* [24] and Quirinale *et al.* [26]. It has been argued that the lower T_N in Sn-flux samples is a result of Co vacancies. However, considering the fact that in our samples there are also Co vacancies and the T_N is as high as that in samples prepared by CoAs self-flux, we think Co vacancies are not the sole reason for the lower T_N; it may also be related to the actual conditions

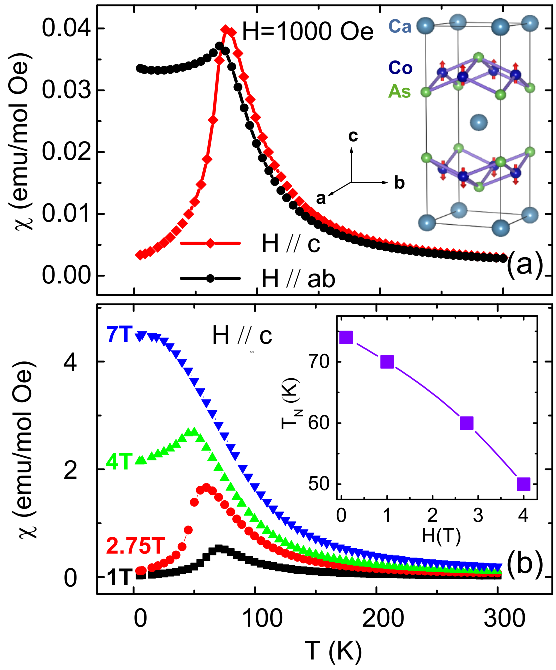

FIG. 2. (Color online) (a) The $M(T)$ curves with $H \parallel c$ (black circle) and $H \parallel ab$ (red diamond) at $H = 0.1$ T. Inset: The unit cell of a $CaCo_2As_2$ single crystal. (b) The $M(T)$ curves in different magnetic fields with $H \parallel c$. Inset: Magnetic field dependence of T_N.

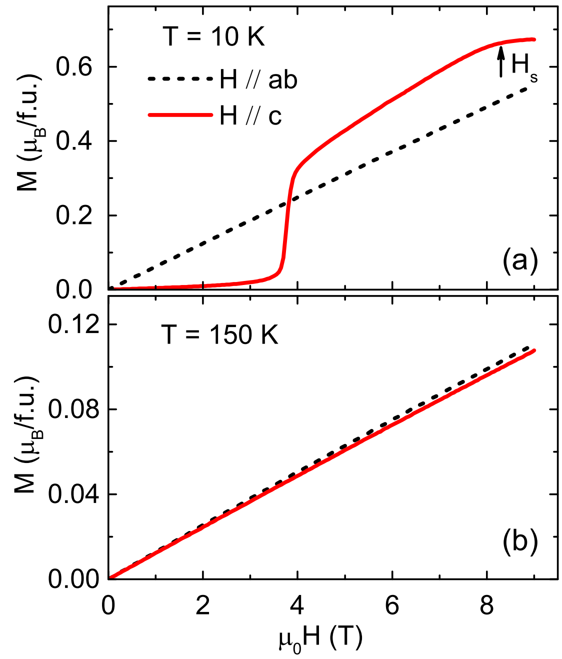

FIG. 3. (Color online) $M(H)$ curves for $H \parallel c$ and $H \parallel ab$ at (a) $T = 10$ K and (b) $T = 150$ K.

in the crystal growth, but more experiments are needed to clarify it. Figure 2(b) shows the FC magnetization in different applied fields. It is obvious that the T_N peak shifts to lower temperature with increasing magnetic field, and it vanishes at 7 T due to suppression of AFM with applied magnetic field, as shown in the inset of Fig. 2(b).

Figures 3(a) and 3(b) show the $M(H)$ curves at $T = 10$ and 150 K for $H \parallel c$ (solid line) and $H \parallel ab$ (dashed line). At $T = 10$ K ($H \parallel c$), the curve shows an AFM feature at low fields, but M suddenly increases around 3.7 T with a sharp step, and finally tends to saturate at above 7.5 T. We attributed the sharp increase in M to the SF transition. We notice that the system shows only one SF transition at 3.7 T. For $H \parallel ab$, M_{ab} increases linearly and no saturation magnetization has been observed with H up to 9 T. Meanwhile, at 150 K, which is well above T_N, the $M(H)$ curves are essentially linear in $H \parallel c$ and $H \parallel ab$ and do not saturate even up to 9 T, as shown in Fig. 3(b).

C. Magnetic torque

In general, the magnetic torque of a paramagnet with an uniaxial anisotropy in SI units takes the following form [33]:

$$\tau_{PM} = \tfrac{1}{2}(\chi_\perp - \chi_\parallel)\mu_0 H^2 \sin 2\theta. \tag{1}$$

For an uniaxial anisotropic antiferromagnet, the free energy F of the system can be expressed as [34–36]

$$F = -\tfrac{1}{2}[\chi_\perp \sin^2(\phi) + \chi_\parallel \cos^2(\phi)]\mu_0 H^2 + K_\mu \sin^2(\phi - \theta). \tag{2}$$

Since torque τ is the angular derivative of free energy F, we get [35–38]

$$\tau_{\text{AFM}} = -\frac{\partial F}{\partial \theta} = \frac{1}{2}(\chi_\perp - \chi_\parallel)\mu_0 H^2 \frac{\sin 2\theta}{\sqrt{\lambda^2 - 2\lambda\cos 2\theta + 1}}. \tag{3}$$

Here, we have

$$\lambda = \left(\frac{H}{H_{SF}}\right)^2, \tag{4}$$

and the SF field

$$H_{SF} = \sqrt{\frac{2K_\mu}{\mu_0(\chi_\perp - \chi_\parallel)}}. \tag{5}$$

There are two terms of the free energy in Eq. (2): the first term is the magnetic energy and the second is the anisotropy energy, $\chi_\perp$ and $\chi_\parallel$ are the spin susceptibilities perpendicular and parallel, respectively, to the magnetization easy axis, ϕ is the angle between the applied magnetic field and spin axis, θ is the angle between the applied magnetic field and the easy axis, μ_0 is the vacuum magnetic permeability, and K_μ is the anisotropy energy.

Figure 4(a) shows the magnetic torque curves at different applied field direction θ at $T = 10$ K. θ is the angle between magnetic field H and the c axis. It shows a sharp dip for $\theta > 0^\circ$ which changes to a peak for $\theta < 0^\circ$ at H_{SF}. When $H > H_{SF}$, the system changes to a SF phase and the torque amplitude decreases and shows a sign change with increasing H. With further increasing H, $\tau(H)$ curves deviate from their trend in higher field and tend to saturate. We attributed this tendency of saturation at H_S to a separation from SF phases to a PM state. The SF dip becomes broader as θ gets away from zero. Moreover, as shown in the inset of Fig. 4(b), H_{SF}

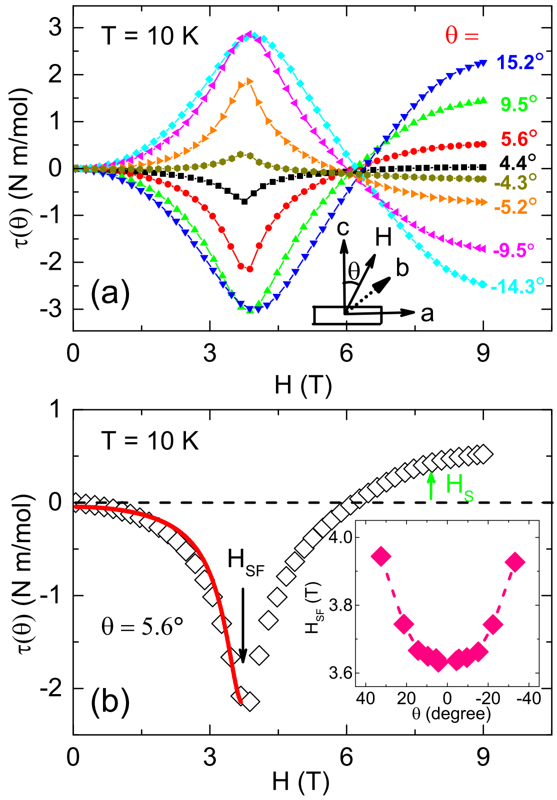

FIG. 4. (Color online) (a) $\tau(H)$ curves of $CaCo_2As_2$ for θ from -14.3° to 15.2° at $T = 10$ K. (b) $\tau(H)$ curve at $\theta = 5.6^\circ$ and the fitting results below H_{SF} by Eq. (3) (red solid line). Inset: Angular-dependent SF transition field H_{SF} at $T = 10$ K.

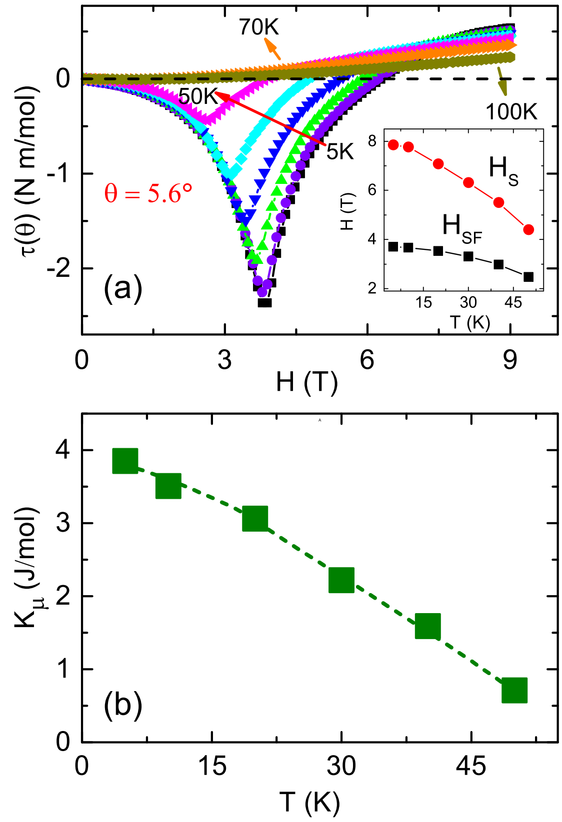

FIG. 5. (Color online) (a) Magnetic field dependence of magnetic torque curves at $\theta = 5.6\ ^\circ$ at different temperatures. Inset: Temperature dependence of H_{SF} and H_{FM} at $T = 5$, 10, 20, 30, 40, and 50 K. (b) T-dependent anisotropic energy K_μ obtained from the fitting result by Eq. (3).

slightly increases with increasing tilting angle θ and shows a minimum when the magnetic field is oriented along the c axis ($H \parallel c$); this feature indicates that the c axis is the easy axis for the ordered Co spins in this system [39].

In order to understand the field-dependent torque, we choose one sharp curve at $\theta = 5.6^\circ$ to analyze in detail. As shown in Fig. 4(b), a dip position (black arrow) and a saturation tendency (green arrow) are observed at $H_{SF} = 3.7$ T and $H_S = 7.7$ T, respectively. Since Eq. (3) is only right when the parallel and perpendicular magnetization are proportional to the applied fields, we fit the experimental $\tau(H)$ curves just below H_{SF} and find that the fitting is almost in agreement with the experimental data. With further increasing field, the observed saturation of the torque signal above H_S is a result of Co spins aligned along the direction of applied fields in high fields. This tendency of saturation is consistent with the results of $M(H)$, as shown in Fig. 3(a).

Next, we will discuss the field dependence of the magnetic torque signal for $\theta \sim 5.6^\circ$ at different temperatures. As shown in Fig. 5(a), both the amplitude of the SF dip and H_{SF} decrease with increasing temperature. At higher temperatures, the magnetic spins fluctuate around their anisotropy axes and smaller field is required for SF transition, and finally the SF dip vanishes above 70 K where a magnetic transition from the AFM to PM state occurs. The AFM to PM transition temperature T_N deduced from $\tau(T)$ curves is consistent with that as determined from $M(T)$. H_S also shows a decreasing trend with increasing temperature as shown in the inset of Fig. 5(a). We have also fitted these $\tau(H)$ curves below H_{SF} by using Eq. (3); the fitted parameters K_μ for different temperatures are plotted in Fig. 5(b). It shows a decreasing trend with increasing temperature due to a decrease in the AFM anisotropy energy with temperature.

Figures 6(a)–6(e) show the angular-dependent torque curves in the temperature region of 10–100 K under different applied fields. It is evident that all of the $\tau(\theta)$ curves with $H = 1$ T exhibit a sinusoidal wave shape and an extremum (maxima or minima) around $\theta = 45^\circ$. The $\tau(\theta)$ curves show a symmetrical behavior at 90°, and therefore we will discuss only the first part that lies in the range $0 \leqslant \theta \leqslant 90^\circ$. The amplitude of the minima decreases with increasing temperature and becomes positive (a sign change) around 70 K, which is consistent with the $T_N = 70$ K at $H = 1$ T as determined from $M(T)$ [Fig. 2(b)]. Therefore, a sign change in the $\tau(\theta)$ curves with increasing temperature is due to the magnetic transition from the AFM to PM state. Similar changes were also observed for $H = 2.75$ T and $H = 4$ T, as shown in Figs. 6(b) and 6(c). However, the minima in these two fields shifts away from $\theta = 45^\circ$ and the sinusoidal wave shape transfers into the sawtooth wave form, which are attributed to the SF transition between 2.75 and 4 T. At $H = 7$ T [Fig. 6(d)], the lower-temperature curves exhibit a very different shape as compared to curves at higher temperature, which can arise from a transition from SF

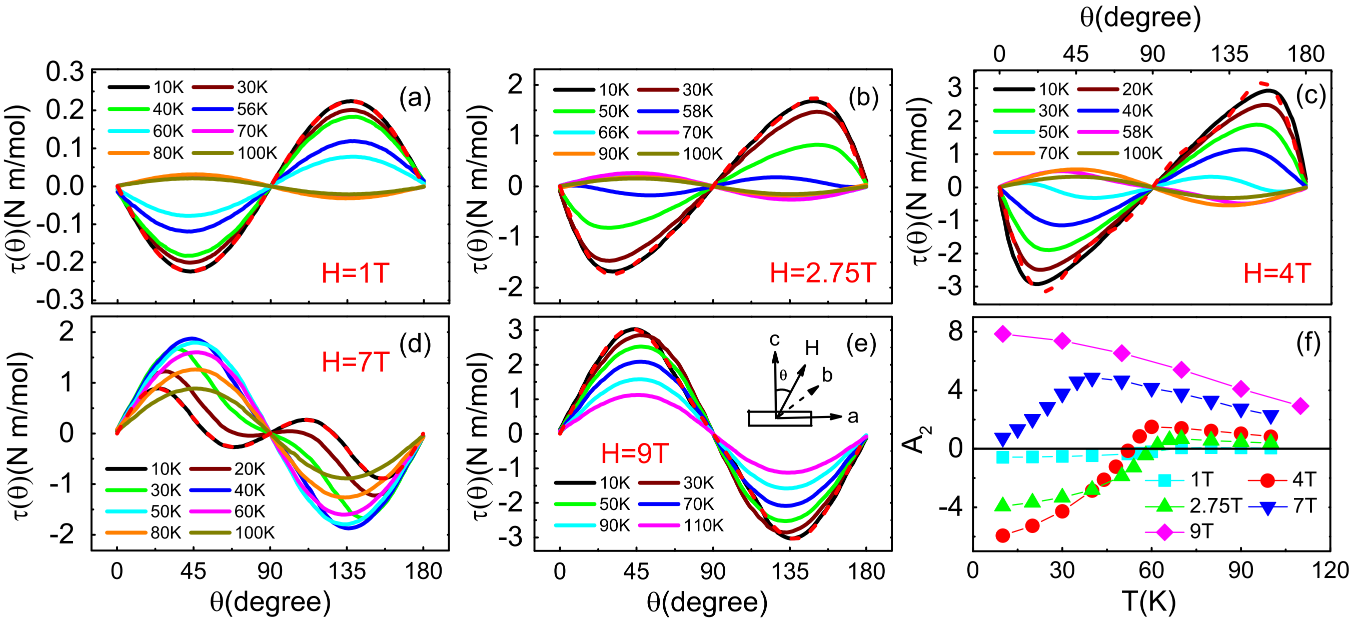

FIG. 6. (Color online) Angular dependence of magnetic torque of a $CaCo_2As_2$ single crystal in different magnetic fields. (a) $H = 1$ T, (b) $H = 2.75$ T, (c) $H = 4$ T, (d) $H = 7$ T, and (e) $H = 9$ T. (f) Temperature dependence of the coefficient A_2 in different magnetic fields. The red dashed lines at $T = 10$ K in each magnetic field are the fitting results with Eq. (6).

phases to a PM state. On further increasing magnetic field to 9 T [Fig. 6(e)], the low-temperature $\tau(\theta)$ curve at 10 K exhibits only a positive peak in $0 \leqslant \theta \leqslant 90^\circ$ because the system is in the field-induced saturated PM state at 9 T. The amplitude of the peak in $\tau(\theta)$ curves decreases with increasing temperature, but exhibits only positive $\tau(\theta)$ in the whole temperature region ($10 \leqslant T \leqslant 100$ K). The decrease of peak amplitude with temperature is due to increasing thermal fluctuations at high temperature which disturb the Co spins of the saturated PM. The magnetic transitions from AFM to PM, as determined from $\tau(\theta)$ analysis, are in agreement with the $M(T)$ results.

The angular-dependent magnetic torque can be expanded as [3]

$$\tau = A_2 \sin 2\theta + A_4 \sin 4\theta + A_6 \sin 6\theta + \cdots , \quad (6)$$

where the first term is the first-order contribution as described in Eq. (1), and the second and third terms are higher-order corrections. The magnetic torque measured as a function of angle at different fields is fitted by Eq. (6) [the red dashed line at $T = 10$ K in Figs. 6(a)–6(e)]. The typical fitting results of A_2 are shown in Fig. 6(f). For applied fields between 1 and 4 T, as the temperature increases, A_2 shows a sign change because of the magnetic transition from AFM to PM. The transition temperature decreases with increasing field and shifts from 70 to 54 K as the field increases from 1 to 4 T, which is in agreement with the dc magnetization results [Fig. 2(b)].

Figure 7 summarizes the detailed magnetic phase diagram of a $CaCo_2As_2$ single crystal as derived from magnetization (circles) and magnetic torque (diamonds) measurements. We define the following terms: $H_{SF}$is the SF onset field corresponding to the rapid increase in $M(H)$ at $H \parallel c$ and the dip position in $\tau(H)$ curves at $\theta = 5.6$ °; the AFM transition temperature is extracted from the $\chi(T)$ and $\tau(T)$ data. As shown in the phase diagram, below T_N, the magnetic structure is a collinear A-type AFM at low field. With increasing magnetic field, the SF transition occurs at H_{SF} and then all Co spins tend to align along the direction of the external field above H_S. The arrows in the phase diagram represent the corresponding collinear AFM structure, SF phases, and the arrangement of Co moments above H_S, respectively. Meanwhile, above H_S, as the temperature increases, the Co moments will be disturbed by the increasing thermal fluctuation at high temperature and the system may have a gradual variation to the unsaturated PM state. Through a combination of magnetization and magnetic torque measurements, we provide a detailed and systematical

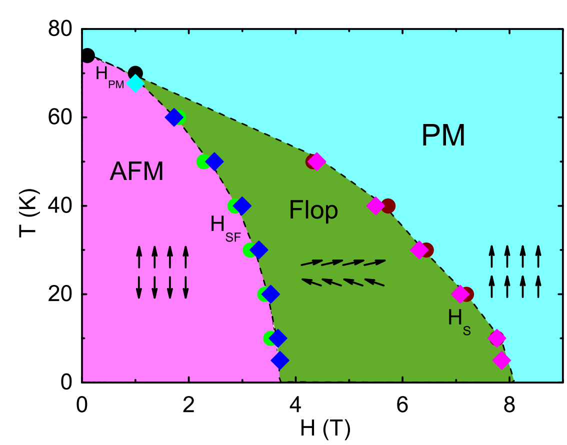

FIG. 7. (Color online) T-H phase diagram concluded from magnetization (circles) at $H \parallel c$ and magnetic torque (diamonds) measurements at $\theta = 5.6^\circ$ for $CaCo_2As_2$. The curves are guides to the eye. The collinear AFM structure, SF phases, and the arrangement of Co moments above H_S with $H \parallel c$ are shown with the corresponding arrows in the figure.

way to analyze the metamagnetic transition, especially the spin-flop transition.

IV. CONCLUSIONS

In conclusion, we have systematically investigated the magnetic properties of a $CaCo_2As_2$ single crystal through dc magnetization and torque magnetometry. An A-type AFM ground state with $T_N = 74$ K and with easy axis aligned along the c axis are inferred from magnetization and magnetic torque measurements. For $H \parallel c$, the $M(H)$ and $\tau(H)$ data reveal a spin-flop transition below T_N. Together with magnetization measurements, a more detailed analysis of the spin-flop transition and magnetic phase diagram is given by torque measurements.

ACKNOWLEDGMENTS

This research was supported by the Natural Science Foundation of China (Grants No. 11104335, No. 91121004, No. 11274237, No. 51228201, and No. 11004238) and the Ministry of Science and Technology of China (973 Projects No. 2009CB929102, No. 2011CBA00107, No. 2012CB821400, No. 2012CB921302, and No. 2015CB921303). The authors also acknowledge the support of the Priority Academic Program Development of Jiangsu Higher Education Institutions (PAPD).

[1] L. Néel, Proc. Phys. Soc. A **65**, 869 (1952).
[2] T. Fries, Y. Shapira, F. Palacio, M. C. Morón, G. J. McIntyre, R. Kershaw, A. Wold, and E. J. McNiff, Phys. Rev. B **56**, 5424 (1997).
[3] H. Uozaki, T. Sasaki, S. Endo, and N. Toyota, J. Phys. Soc. Jpn. **69**, 2759 (2000).
[4] T. Sasaki, H. Uozaki, S. Endo, and N. Toyota, Synth. Metals **120**, 759 (2001).
[5] W. Wernsdorfer, N. Aliaga-Alcalde, D. N. Hendrickson, and G. Christou, Nature (London) **416**, 406 (2002).
[6] T. Kawamoto, Y. Bando, T. Mori, T. Konoike, Y. Takahide, T. Terashima, S. Uji, K. Takimiya, and T. Otsubo, Phys. Rev. B **77**, 224506 (2008).
[7] M. R. Fitzsimmons, P. Yashar, C. Leighton, I. K. Schuller, J. Nogués, C. F. Majkrzak, and J. A. Dura, Phys. Rev. Lett. **84**, 3986 (2000).
[8] M. Reehuis and W. Jeitschko, J. Phys. Chem. Solids **51**, 961 (1990).
[9] M. Reehuis, P. Brown, W. Jeitschko, M. Mller, and T. Vomhof, J. Phys. Chem. Solids **54**, 469 (1993).
[10] M. Reehuis, C. Ritter, R. Ballou, and W. Jeitschko, J. Magn. Magn. Mater. **138**, 85 (1994).
[11] M. Reehuis, W. Jeitschko, G. Kotzyba, B. Zimmer, and X. Hu, J. Alloys Compd. **266**, 54 (1998).
[12] M. Rotter, M. Tegel, D. Johrendt, I. Schellenberg, W. Hermes, and R. Pöttgen, Phys. Rev. B **78**, 020503 (2008).
[13] M. Rotter, M. Tegel, and D. Johrendt, Phys. Rev. Lett. **101**, 107006 (2008).
[14] C. de la Cruz, Q. Huang, J. W. Lynn, J. Li, W. Ratcliff II, J. L. Zarestky, H. A. Mook, G. F. Chen, J. L. Luo, N. L. Wang, and P. Dai, Nature (London) **453**, 899 (2008).
[15] R. M. Fernandes, D. K. Pratt, W. Tian, J. Zarestky, A. Kreyssig, S. Nandi, M. G. Kim, A. Thaler, N. Ni, P. C. Canfield, R. J. McQueeney, J. Schmalian, and A. I. Goldman, Phys. Rev. B **81**, 140501 (2010).
[16] Z. Shermadini, A. Krzton-Maziopa, M. Bendele, R. Khasanov, H. Luetkens, K. Conder, E. Pomjakushina, S. Weyeneth, V. Pomjakushin, O. Bossen, and A. Amato, Phys. Rev. Lett. **106**, 117602 (2011).
[17] I. I. Mazin, D. J. Singh, M. D. Johannes, and M. H. Du, Phys. Rev. Lett. **101**, 057003 (2008).
[18] J. K. Dong, S. Y. Zhou, T. Y. Guan, H. Zhang, Y. F. Dai, X. Qiu, X. F. Wang, Y. He, X. H. Chen, and S. Y. Li, Phys. Rev. Lett. **104**, 087005 (2010).
[19] M. S. Torikachvili, S. L. Bud'ko, N. Ni, and P. C. Canfield, Phys. Rev. Lett. **101**, 057006 (2008).
[20] A. Kreyssig, M. A. Green, Y. Lee, G. D. Samolyuk, P. Zajdel, J. W. Lynn, S. L. Bud'ko, M. S. Torikachvili, N. Ni, S. Nandi, J. B. Leão, S. J. Poulton, D. N. Argyriou, B. N. Harmon, R. J. McQueeney, P. C. Canfield, and A. I. Goldman, Phys. Rev. B **78**, 184517 (2008).
[21] A. I. Goldman, A. Kreyssig, K. Prokeš, D. K. Pratt, D. N. Argyriou, J. W. Lynn, S. Nandi, S. A. J. Kimber, Y. Chen, Y. B. Lee, G. Samolyuk, J. B. Leão, S. J. Poulton, S. L. Bud'ko, N. Ni, P. C. Canfield, B. N. Harmon, and R. J. McQueeney, Phys. Rev. B **79**, 024513 (2009).
[22] S. R. Saha, N. P. Butch, T. Drye, J. Magill, S. Ziemak, K. Kirshenbaum, P. Y. Zavalij, J. W. Lynn, and J. Paglione, Phys. Rev. B **85**, 024525 (2012).
[23] N. Ni, S. Nandi, A. Kreyssig, A. I. Goldman, E. D. Mun, S. L. Bud'ko, and P. C. Canfield, Phys. Rev. B **78**, 014523 (2008).
[24] B. Cheng, B. F. Hu, R. H. Yuan, T. Dong, A. F. Fang, Z. G. Chen, G. Xu, Y. G. Shi, P. Zheng, J. L. Luo, and N. L. Wang, Phys. Rev. B **85**, 144426 (2012).
[25] J. J. Ying, Y. J. Yan, A. F. Wang, Z. J. Xiang, P. Cheng, G. J. Ye, and X. H. Chen, Phys. Rev. B **85**, 214414 (2012).
[26] D. G. Quirinale, V. K. Anand, M. G. Kim, A. Pandey, A. Huq, P. W. Stephens, T. W. Heitmann, A. Kreyssig, R. J. McQueeney, D. C. Johnston, and A. I. Goldman, Phys. Rev. B **88**, 174420 (2013).
[27] V. K. Anand, R. S. Dhaka, Y. Lee, B. N. Harmon, A. Kaminski, and D. C. Johnston, Phys. Rev. B **89**, 214409 (2014).
[28] P. Canfield and S. Bud'ko, J. Alloys Compd. **262-263**, 169 (1997).
[29] D. G. Naugle, B. I. Belevtsev, K. D. D. Rathnayaka, S.-I. Lee, and S. M. Yeo, J. Appl. Phys. **103**, 07B718 (2008).

[30] X. F. Wang, T. Wu, G. Wu, H. Chen, Y. L. Xie, J. J. Ying, Y. J. Yan, R. H. Liu, and X. H. Chen, Phys. Rev. Lett. **102**, 117005 (2009).
[31] F. Ronning, T. Klimczuk, E. D. Bauer, H. Volz, and J. D. Thompson, J. Phys. Condens. Matter **20**, 322201 (2008).
[32] J. J. Ying, J. C. Liang, X. G. Luo, Y. J. Yan, A. F. Wang, P. Cheng, G. J. Ye, J. Q. Ma, and X. H. Chen, Europhys. Lett. **104**, 67005 (2013).
[33] H. Xiao, T. Hu, C. C. Almasan, T. A. Sayles, and M. B. Maple, Phys. Rev. B **73**, 184511 (2006).
[34] T. Nagamiya, Prog. Theor. Phys. **6**, 342 (1951).
[35] K. Yosida, Prog. Theor. Phys. **6**, 691 (1951).
[36] T. Nagamiya, K. Yosida, and R. Kubo, Adv. Phys. **4**, 1 (1955).
[37] S. Weyeneth, P. J. W. Moll, R. Puzniak, K. Ninios, F. F. Balakirev, R. D. McDonald, H. B. Chan, N. D. Zhigadlo, S. Katrych, Z. Bukowski, J. Karpinski, H. Keller, B. Batlogg, and L. Balicas, Phys. Rev. B **83**, 134503 (2011).
[38] M. D. Watson, A. McCollam, S. F. Blake, D. Vignolles, L. Drigo, I. I. Mazin, D. Guterding, H. O. Jeschke, R. Valenti, N. Ni, R. Cava, and A. I. Coldea, Phys. Rev. B **89**, 205136 (2014).
[39] X. Xu, A. Carrington, A. I. Coldea, A. Enayati-Rad, A. Narduzzo, S. Horii, and N. E. Hussey, Phys. Rev. B **81**, 224435 (2010).